The Egyptian Journal of Remote Sensing and Space Sciences 21 (2018) 345–351

HOSTED BY

Contents lists available at ScienceDirect

The Egyptian Journal of Remote Sensing and Space Sciences

journal homepage: www.sciencedirect.com

Research Paper

Unsupervised change detection in remote sensing images using fusion of spectral and statistical indices

Akansha Singh [a,*], Krishna Kant Singh [b]

[a] SCSE, Galgotias University, Greater Noida, India
[b] ECE, GL Bajaj Institute of Technology and Management, Greater Noida, India

ARTICLE INFO

Article history:
Received 19 April 2017
Revised 20 January 2018
Accepted 28 January 2018
Available online 7 February 2018

Keywords:
Change detection
Remote sensing
Kullback Leibler
Wavelets

ABSTRACT

Satellite images are being widely used for change detection applications like urban planning, vegetation monitoring, forest cover management, disaster mitigation and management. There are certain challenges in using these satellite images for change detection. Firstly, the heterogeneity in image acquisition at different times, secondly the volume of information contained in these images and lastly mixed pixel problem. The existing methods make use of spectral features of the images to detect changes as they are a good measure of identifying changes. When the incidence angle during image acquisition is different the spectral features vary whereas the statistical distribution of the pixels remains uniform. Therefore, in this paper a novel method is proposed that takes into account both spectral and statistical features while detecting changes. The spectral changes are recorded using change vector analysis and the statistical changes are identified using a similarity index based on Kullback Leibler distance. The spectral change information and the similarity index are fused using wavelets. The fused image is classified into change and unchanged classes using a neuro fuzzy classifier that overcomes the mixed pixel problem of satellite images while keeping the classification optimal. Experimental results show that the proposed method gives accurate results.

1. Introduction

Change detection plays a pivotal role in sustainable development of human society. Environmental monitoring and planning makes use of this technology for understanding the global changes and natural impacts on land surface. Change detection methods find the changes over a geographical area with the use of bitemporal images of the area. Numerous earth observing satellites are now functional that have revisit property. This revisit property helps researchers to obtain satellite imagery of a geographical area on different times. The different spectral features of these images are correlated to changes on the land cover. The commonly used procedure involves creating a difference image and then classifying this into a binary change map. In the literature, the subtraction operation and ratio operation are two basic tools for producing the difference image. Some methods use a single difference image (Bruzzone and Prieto, 2000; Ertürk and Plaza, 2015; Chatelain et al.,2008; Celik and Ma,2010; Celik and Ma, 2011; Çelik, 2011) while others fuse more than one difference images to obtain complimentary information. These methods classify the images into changed and unchanged classes. The classified images are further compared to detect changes. The latest versions of these include mean-filtered subtraction (Zheng et al., 2014), log-ratio, and mean-ratio (Gong et al., 2012). In Gong et al., a mean-ratio image and a log-ratio image are fused. It illustrates that, for synthetic aperture radar (SAR) images, the mean-ratio image enhances the information of changed regions and the log-ratio image restrains the background information. Therefore, fusing the two images provides better performance (Gong et al., 2012). Bovolo et al. (2008) proposed a semi-supervised support vector machine based method. This method works in two phases, in the first phase a training set is created using CVA and Bayesian thresholding. The training sets are used to create a change map showing changed and unchanged areas.

Another method employs Gaussian mixture model and Bayes theory for identifying changes in bi-temporal images. The difference image is first modeled with Gaussian mixture model and is then classified into changed and unchanged classes using Bayes theory (Celik, 2010). Bovolo et al. (2012) proposed a change

Peer review under responsibility of National Authority for Remote Sensing and Space Sciences.

* Corresponding author.
E-mail address: akanshasing@gmail.com (A. Singh).

https://doi.org/10.1016/j.ejrs.2018.01.006
1110-9823/

detection method, in which a feature space is created from the available spectral changes. The final changes are identified using the Expectation Maximization algorithm. Du et al. (2013) introduced a decision level fusion based method for change detection. The authors fused multiple difference images like subtraction, ratio, absolute Euclidean distance, and chi-square transformation to obtain the change map. Change detection techniques based on unsupervised classification are also available in the literature (Singh et al., 2014). In Zheng et al., a mean-filtered subtraction image and a median-filtered log-ratio image are fused for SAR image change detection. They state that the joint use of the two difference images can produce a smooth change map and preserve well edges of changed areas simultaneously (Zheng et al., 2014). A recent approach uses wavelet kernels for fusing two difference images to obtain the change map. The subtraction operation and ratio operation are applied on bitemporal images. The change information obtained from both the operations are fused using wavelet kernels (Jia et al., 2016). Recently, Superresolution change detection method (SRCD) method is proposed that uses end member estimation, spectral unmixing, land-cover fraction change detection, and superresolution land-cover mapping (Li et al., 2016). The methods discussed above concentrate on detecting the changes using spectral features while some make use of statistical distribution of pixels. In both cases some changes remain unattended and thus the accuracy of the methods degrades. In situations where the incidence angle or the illumination conditions vary at the time of image acquisition, the bitemporal images have different spectral features.

The available state of the art methods do not use fusion of spectral and statistical information. In this paper, a novel method that fuses spectral and statistical information is presented. Spectral features are a good measure for obtaining change information, but in cases when images are not acquired from the same incidence angle some change information is lost. However the statistical distribution of pixels remains constant and independent of the incidence angle. Thus, using similarity index along with spectral features gives complete and accurate change information between two images. Therefore the proposed method, computes the changes based on spectral features using CVA and the statistical distribution is analyzed using a similarity index based on Kullback Leibler distance. Wavelets Fusion is used to fuse these two indices to obtain complete change information. The fused image is further clustered into changed and unchanged classes using a neuro fuzzy classifier RBF/GIFP-FCM classifier. The experiments are done on three different datasets to analyze the performance of the method. The method was also compared with the other existing state of the art methods.

2. Methodology

The flowchart of the proposed method is shown in Fig. 1. Let us consider two bi-temporal images I_1 and I_2 , acquired on time t_1 and t_2 over the same geographical area. The aim is to achieve a change map C_m, highlighting the change areas. The various steps involved are discussed as follows:

2.1. Similarity index using Kullback Leibler divergence

The similarity index is computed to analyze the change in the statistics of each pixel. In KLD the divergence between the probability density functions is analyzed. KLD is based on the use of information theoretical similarity measures (Bujor et al., 2004). The divergence is a function of two probability densities characterizing a random variable that describes the image behaviors in the local neighborhood of the analyzed pixel. If the probability densities are similar (no change), the Kullback-Leibler divergence has a small value otherwise the value is high. If a pixel is changed then its statistical distribution is also changed whereas if a pixel remains unchanged then its statistical distribution also remains unchanged. This change can be quantified using a scalar change index that measures the statistical distributions and therefore KLD is used. Let us consider two images I_1 and I_2 taken at times t_1 and t_2 respectively. While computing the similarity index the spectral values in different bands do not affect the result thus a single band is used for computing KLD. In this paper the first band is used however the choice of another band will not affect the similarity index. As the similarity index depends on the statistical distribution of pixels therefore the spectral values in different bands may be different but the statistical distribution in all bands is similar. Thus, any band can be considered while computing the similarity index. The similarity index is computed as follows.

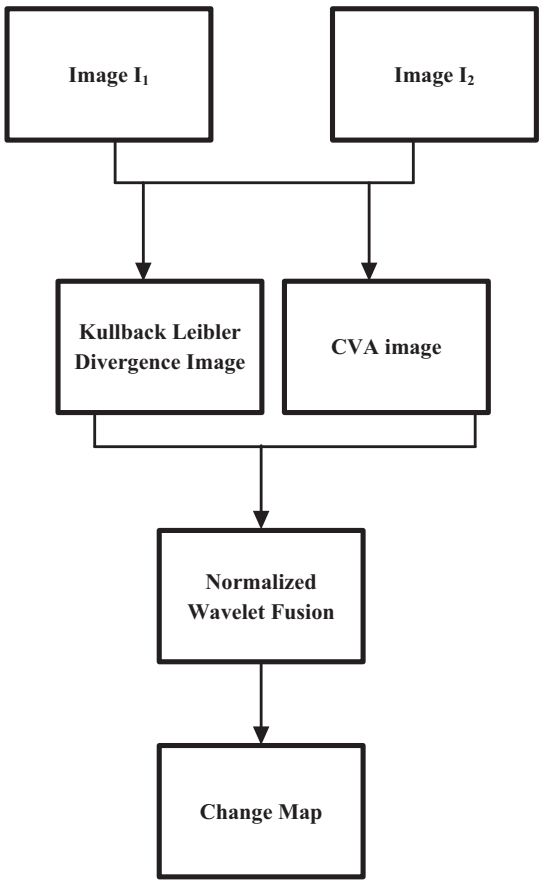

Fig. 1. Flowchart of the proposed method.

The Kullback-Leibler divergence between these images can be computed using Eq. (1).

$$SI_{KL}(I_1/I_2) = \int^{l} og\left[\frac{p(I_1)}{p(I_2)}\right] p(I_1). \quad (1)$$

In case of images we consider discrete probability laws, defined on finite set of points thus Eq. (1) for discrete points can be written as

$$SI_{KL}(I_1/I_2) = \sum_i log\left[\frac{p(\{x_{i1}\})}{p(\{x_{i2}\})}\right] p(\{x_{i1}\}). \quad (2)$$

Where x_{ik} represents the i^{th} point in the k^{th} image. The probabilities are calculated using the neighborhood pixels, in this paper a neighborhood window of size 3×3 is used. $SI_{KL}(I_1/I_2)$, is a measure

of divergence from I_1 to I_2. This measure is not symmetric thus $SI_{KL}(I_1/I_2) \neq SI_{KL}(I_2/I_1)$. The symmetric version of this can be defined as:

$$SI_{KLD}(I_1, I_2) = I_{KL}(I_1/I_2) + I_{KL}(I_2/I_1). \quad (3)$$

SI_{KLD} is the similarity index based on KLD. The output image SI_{KLD} obtained will appear dark in areas of no change and bright in changed areas.

2.2. Spectral change index

The spectral change index detects changes based on the spectral value of pixels. The images are multispectral thus to encompass changes from all the layers CVA is used for computing the spectral change index. CVA works on multiple bands and creates a single band image containing change information (Johnson and Kasischke,1998). The spectral change index is computed using Eq. (4).

$$SCI_{cva}(i,j) = \sqrt{\sum_{b=1}^{m} (I_{1_{(i,j)_b}} - I_{2_{(i,j)_b}})^2} \quad (4)$$

where m is the number of bands, $SCI_{cva}(i,j)$ is the pixel at location (i, j) of the CVA image, $I_{1_{(i,j)_b}}$ and $I_{2_{(i,j)_b}}$ represent the pixel at location (i,j) of b^{th} band of the images I_1 and I_2 respectively. The SCI_{cva} has higher values and appears brighter at locations where changes have occurred while has low values and appears darker at locations where no changes have occurred.

2.3. Fusion of similarity and spectral change indices

Image fusion is a technique that combines information from different sources resulting in a fused image with large amount of information. With image fusion the strengths of different sources are combined together to obtain an improved image with better visual quality suited for image interpretation (Pohl and Van Genderen,1998). The change information obtained from SI_{KL} and SCI_{cva} are combined using fusion. A number of fusion techniques are available in the literature that is used to combine information from different images. Discrete Wavelet Transform (DWT) is being widely used for image fusion. DWT performs a multi resolution analysis of the images in both spatial and temporal domain resulting in a much more detailed information image (Bruzzone and Prieto, 2000). DWT is appropriate for applications like image compression but when used for image analysis DWT does not provides optimal solution. The reason for this is that DWT is not translation invariant and thus produces a large number of artifacts in the reconstructed image. Thus, for image analysis Undecimated Discrete Wavelet transform (UDWT) is quite suitable (Starck et al.,2007). UDWT uses the same filter bank as DWT but does not perform downsampling therefore each subband of UDWT is of the same size as the original image. The reconstructed image is less sensitive to noise, shift invariant and does not has aliasing problem since there is no down sampling. The multiresolution analysis of an image I using UDWT decompositions is a two-step process .Firstly, k- level UDWT decompositions of the image is done. At each level four subbands are created denoted by $I_{k,ll}$, $I_{k,lh}$, $I_{k,hl}$ and $I_{k,hh}$ where $k = 1, 2, \ldots s$. $I_{k,ll}$ is the low frequency subband obtained by performing the low pass filtering (l) along the rows and then along the columns. The other three are high frequency subbands obtained by first applying high pass (h) filter or low pass filter (l) along the rows and then applying high pass (h) filter or low pass filter (l) along the columns. Finally, inverse UDWT is applied to reconstruct the original image by applying the steps of UDWT in reverse order. The UDWT decompositions can be computed using Eq. (5) to Eq. (8),

$$I_{k+1,ll}(i,j) = \sum_{m=0}^{N_{k,l-1}} \sum_{n=0}^{N_{k,l-1}} l_k(m) l_k(n) I_{k,ll}(i+m, j+n). \quad (5)$$

$$I_{k+1,lh}(i,j) = \sum_{m=0}^{N_{k,l-1}} \sum_{n=0}^{N_{k,h-1}} l_k(m) h_k(n) I_{k,ll}(i+m, j+n). \quad (6)$$

++

$$I_{k+1,hl}(i,j) = \sum_{m=0}^{N_{k,h-1}} \sum_{n=0}^{N_{k,l-1}} h_k(m) l_k(n) \mathrm{I}_{k,ll}(i+m, j+n). \quad (7)$$

$$I_{k+1,hh}(i,j) = \sum_{m=0}^{N_{k,h-1}} \sum_{n=0}^{N_{k,h-1}} h_k(m) h_k(n) \mathrm{I}_{k,ll}(i+m, j+n). \quad (8)$$

where $N_{k,l}$ and $N_{k,h}$ are the lengths of the low-pass filter l_k and the high pass filter h_k, $I_{0,ll} = I$. SCI_{cva}

One level UDWT decomposition of an image is shown in Fig. 2.

The change information is combined using wavelet fusion rule (Celik, 2010). The two difference indices and SI_{KLD} obtained from Eqs. (1) and (2) contain change information, this information is combined to obtain a more accurate change image using wavelet fusion rule given in Eq. (9). On applying the UDWT decompositions of SCI_{cva} and SI_{KLD} using Eq. (5) to Eq. (8) four sub bands of each are obtained. The low-frequency subband represents the profile features of the source image; it can significantly reflect the information of changed regions of two images. Thus, the low frequency subband images are fused together using the fusion rule presented here. The results of fusion also depend upon the level of decomposition, it is not necessary that more number of decomposition levels will give better results rather they can produce distortions since the features may overlap in lower resolution images. Therefore, based on the spatial extent of the features present in the image the decomposition level should be chosen. In this paper single level decomposition is done. The low level coefficients of the two difference images are denoted by SI_{ll}^{KLD} and SCI_{ll}^{cva} are fused together using Eq. (10).

$$I_{fu} = \eta SI_{ll}^{KLD} + \nu SCI_{ll}^{cva}. \quad (9)$$

$$\eta = \frac{\min(|SI_{ll}^{KLD}|, |\overline{\mathrm{I}_{ll}}|)}{\max(|SI_{ll}^{KLD}|, |\overline{\mathrm{I}_{ll}}|)} \quad (10)$$

$$\nu = 1 - \eta \quad (11)$$

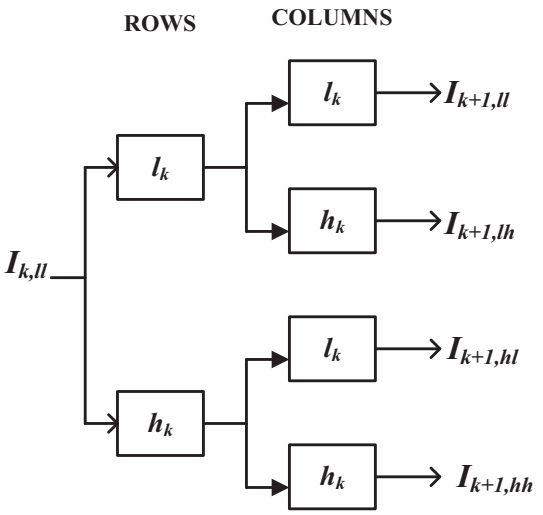

Fig. 2. Undecimated Discrete Wavelet Transform.

$$\overline{I_{ll}} = \frac{(SI_{ll}^{KLD} + SCI_{ll}^{cva})}{2} \tag{12}$$

where I_{fu} is the fused image, $\overline{I_{ll}}$ is the mean value of low frequency coefficients of Similarity index (SI_{ll}^{KLD}) and Spectral change index (SCI_{ll}^{cva}). The low frequency sub bands of SCI_{cva} and SI_{KLD} contain complementary information, i.e., some changes that are visible in one image may not be present in the other image and vice versa thus fusing these images gives complete change information. The parameters η and ν are used to balance the wavelet coefficients of the images. Normalization of η and ν aligns the value of the wavelet coefficients to a common scale, so that the fused image does not have extreme values.

2.4. Clustering using RBF/GIFP-FCM

The fused image, I_{fu} contains change information. The next step is to classify this image into changed and unchanged class. The classification is done using RBF/GIFP-FCM network (Mehrotra et al., 2015). The network computes h cluster centers for classifying the input image into h classes. In change detection the number of classes is two thus $h = 2$.

Step 1: *Initialization:* The network parameters and the cluster centers are also initialized to random values. The weights are initialized randomly with a uniform distribution around 0 and with an empirical variance set at 0.02.

Step 2: *Centre Computation:* The centers are computed using GIFP-FCM as given in Eqs. (13) and (14).

$$c_j = \sum_{i=1}^{k} u_{ji}^{m} x_i / \sum_{i=1}^{k} u_{ji}^{m}. \tag{13}$$

where x_i denotes the i_{th} pixel of the input image X, c_j is the jth cluster center, u_{ji} represents the fuzzy membership matrix $U = [\ u_{ji}\ ]$ given by Eq. (14)

$$u_{ji} = 1 / \sum_{l=1}^{h} \left(\frac{d^2(x_i, c_j) - \beta_i}{d^2(x_i, c_l) - \beta_i} \right)^{\frac{1}{m-1}}. \tag{14}$$

where $\beta_i = \alpha \min\{d^2(x_i, c_s) | s \in \{1, 2, \ldots, h\}\}$, for $(0 \leqslant \alpha \leqslant 1)$.

Step 3: *Training:* The Radial basis function network is trained using Eqs. (15)–(17).

$$w_j(t+1) = w_j(t) + \eta_1 \xi(t) \varphi(||\chi(t) - c_j(t)||). \tag{15}$$

$$c_j(t+1) = c_j(t) + \eta_2 \frac{w_j(t)\xi(t)}{\sigma_j^2(t)} \times \varphi(||\chi(t) - c_j(t)||)(\chi(t) - c_j(t)). \tag{16}$$

The width of the node is updated using Eq. (17)

$$\sigma_j(t+1) = \sigma_j(t) + \eta_3 \frac{w_j(t)\xi(t)}{\sigma_j^3(t)} \times \varphi(||\chi(t) - c_j(t)||)||\chi(t) - c_j(t)^2||. \tag{17}$$

where η_1, η_2 and η_3 are the learning rates of weights, centers and standard deviation, the input vector $\chi(t) = \{x_1, x_2, x_3, \ldots, x_N\}$, $||\ ||$ is the Euclidean distance between the input and the jth center, $\varphi_j = \varphi(\frac{\chi - c_j(t)^2}{\sigma_j^2})$ is the RBF function and $\sigma_j = \frac{d_{max}}{h}$ is the standard deviation of the jth Gaussian function. d_{max} is the maximum distance between the centers and h is the number of centers.

Step 4: *Termination Condition:* The network is terminated when the network converges to a stable value. The objective function is given by Eq. (18)

$$E_t(q) = \sum_{t=1}^{T} \sum_{h=1}^{H} \xi(t) \tag{18}$$

where

$$\xi(t) = \frac{1}{2}(d(t) - y(t))^2 \tag{19}$$

where t is the index of training,i.e., iteration number,T is the total number of training cycles, h is the output of the h_{th} layer, d(t) is the desired output and y(t) is the obtained output, q is the index of training patterns. When the condition given in Eq. (20) is met then the procedure is stopped. Otherwise the iteration count is incremented and the operation goes back to Step 2.

$$\frac{E_t(q+1) - E_t(q)}{E_t(q+2) - E_t(q+1)} < \varepsilon \tag{20}$$

The value of ε is generally chosen between 0.5 and 1. In this case the number of clusters is two (changed and unchanged), thus $h = 2$ and the fused images is classified into classes representing changed and unchanged areas.

2.5. Creation of change map

The cluster centers computed using RBF/GIFP-FCM correspond to change and unchanged classes. These are used to cluster the fused image into change and unchanged classes to create a change map. The change map highlights the changed areas whereas unchanged areas are suppressed. All pixels of the fused image, I_{fu} is assigned to one of the two classes based on the Euclidean distance of the pixel.

$$C_m(x, y) = \begin{cases} 1, \|I_{fu} - c_1\| \leqslant \|I_{fu} - c_2\| \\ 0, otherwise \end{cases} \tag{21}$$

c_1: cluster center for change class c_2: cluster center for unchanged class.

Fused image, I_{fu} contains change information.

3. Results and discussion

In this section, the experimental results to demonstrate the validity of the proposed method are presented. The validation is done on three different sets of remote sensing images. Firstly, the result of different steps of the proposed method is shown. Finally, the qualitative and quantitative results of Expectation maximization (EM) based approach (Bruzzone and Prieto, 2000), Markov-random-field (MRF) based method (Bruzzone and Prieto, 2000), Gaussian Mixture Model (GMM) method (Celik, 2010) and the proposed method are analyzed. The results show that the proposed method outperforms the other methods. The proposed method is implemented on Matlab2013a. Three sets of real remote sensing images are shown in Fig. 3. The ground truth images are obtained by manual analysis available as per the details given in table 1.

The information about these images is given in Table 1.

The results of various intermediate steps applied on "Alaska" images are shown in Fig. 4.

The fused image contains much more accurate change information as compared to the single change detection techniques, i.e., CVA and KLD. A comparison of the improvement in change information with respect to the ground truth is given in table 2. TP, TN, FP and FN refer to true positive, true negative, false positive and false negative respectively. Omission error(OE) is the probability that a changed pixel being not identified as changed, Commission error(CE) is the probability that an unchanged pixel is wrongly identified as a changed pixel. The overall accuracy (OA) is computed using the following equation:

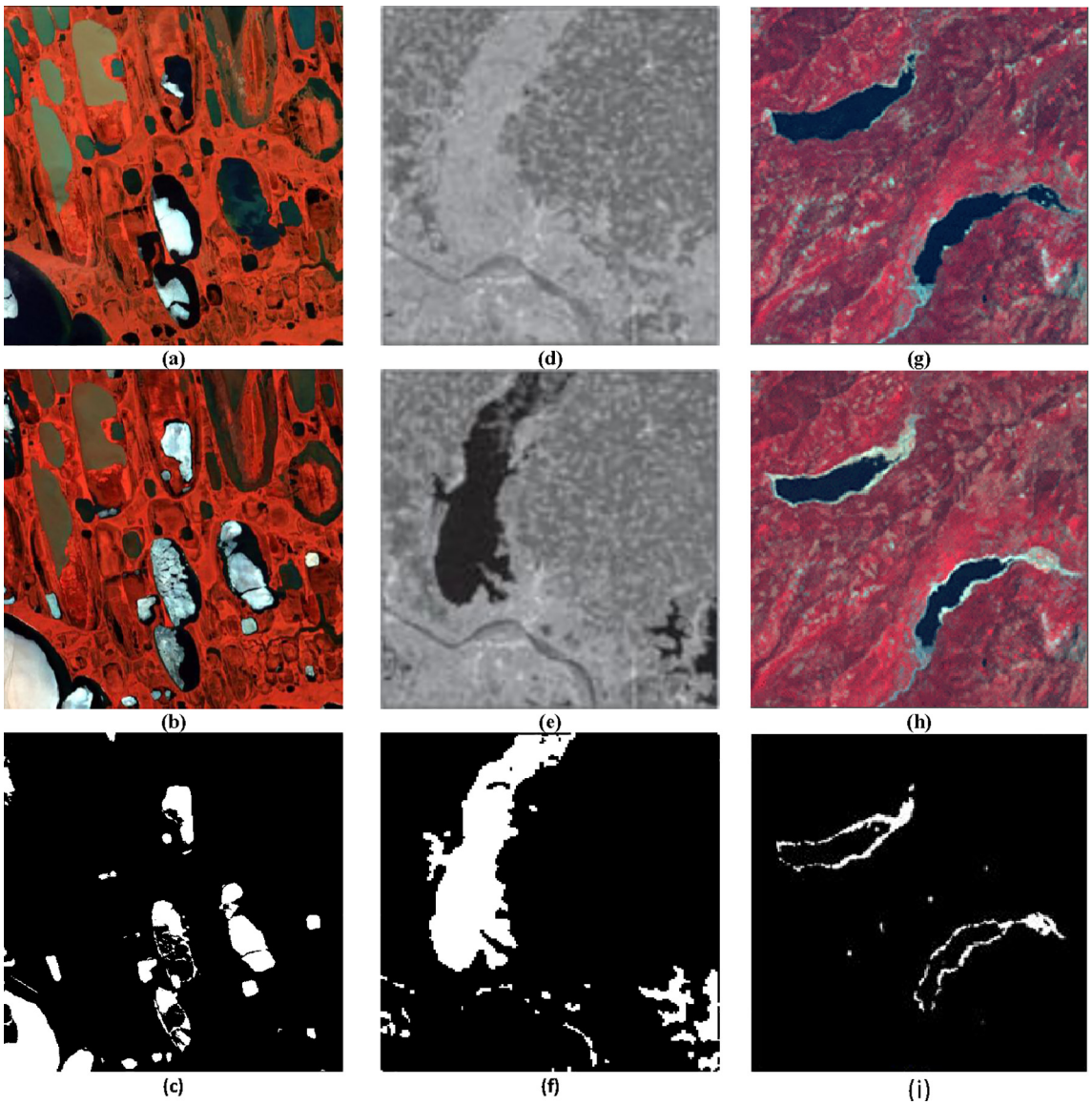

Fig. 3. Satellite images used (a) and (b) bitemporal images "Alaska" (c) Ground truth for "Alaska" (d) and (e) bitemporal images "Bangladesh" (f) Ground truth for "Bangladesh" (g) and (h) bitemporal images "Reno and Lake Tahoe" (i) Ground truth for "Reno and Lake Tahoe".

Table 1
Details of the images used.

Images	Alaska (Image via http://change.gsfc.nasa.gov)	Bangladesh (Image via http://www.esa.int)	Reno and Lake Tahoe (Image via http://geochange.er.usgs.gov)
Sensor	Landsat 5 TM	ASAR	Landsat 5 TM
Resolution	30 *m*	150 *m*	30 *m*
Dates	July 22, 1985	26 July 2007	August 5, 1986
	July 13, 2005	12 April 2007	August 5, 1992
Size	388 × 461	131 × 133	200 × 200
Changes	Snow	Flooding	Drought

$$OA = \frac{TP + TN}{TP + TN + FP + FN}$$

It is observed that the use of fusion led to better results.

The EM, MRF and GMM methods are also implemented on Matlab2013a. These methods are also applied on the datasets given in Table 1. The results of various methods are shown in Fig. 5. Fig. 5 (a)–(c) shows the change map for the three sets of satellite images obtained on applying the EM based approach. In this method, the difference image is analyzed using a threshold value that is automatically selected. This improves the accuracy of the method and reduces the error rate. The results obtained using MRF based method are shown in Fig. 5(d)–(f). This method analyzes the difference image with the spatial contextual information from the neighborhood (Bruzzone and Prieto, 2000). Fig. 5(g)–(i) shows

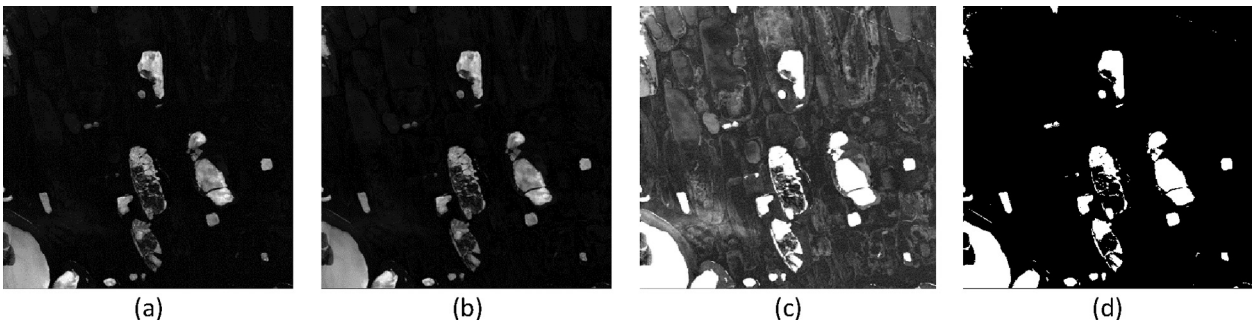

Fig. 4. Result of intermediate steps (a) CVA image (b) Kullback Leibler Distance image (c) Fused image (d) Change map obtained after clustering.

Table 2
Performance of single versus fused change image.

Image	Method	TP	TN	FP	FN	OE (%)	CE (%)	OA (%)
ALASKA	CVA	13,996	160,302	2657	1913	12.02	1.63	97.45
	KL Divergence	13,973	161,325	1634	1936	12.17	1.00	98.00
	Fused	15,303	161,997	840	876	5.41	0.52	99.04

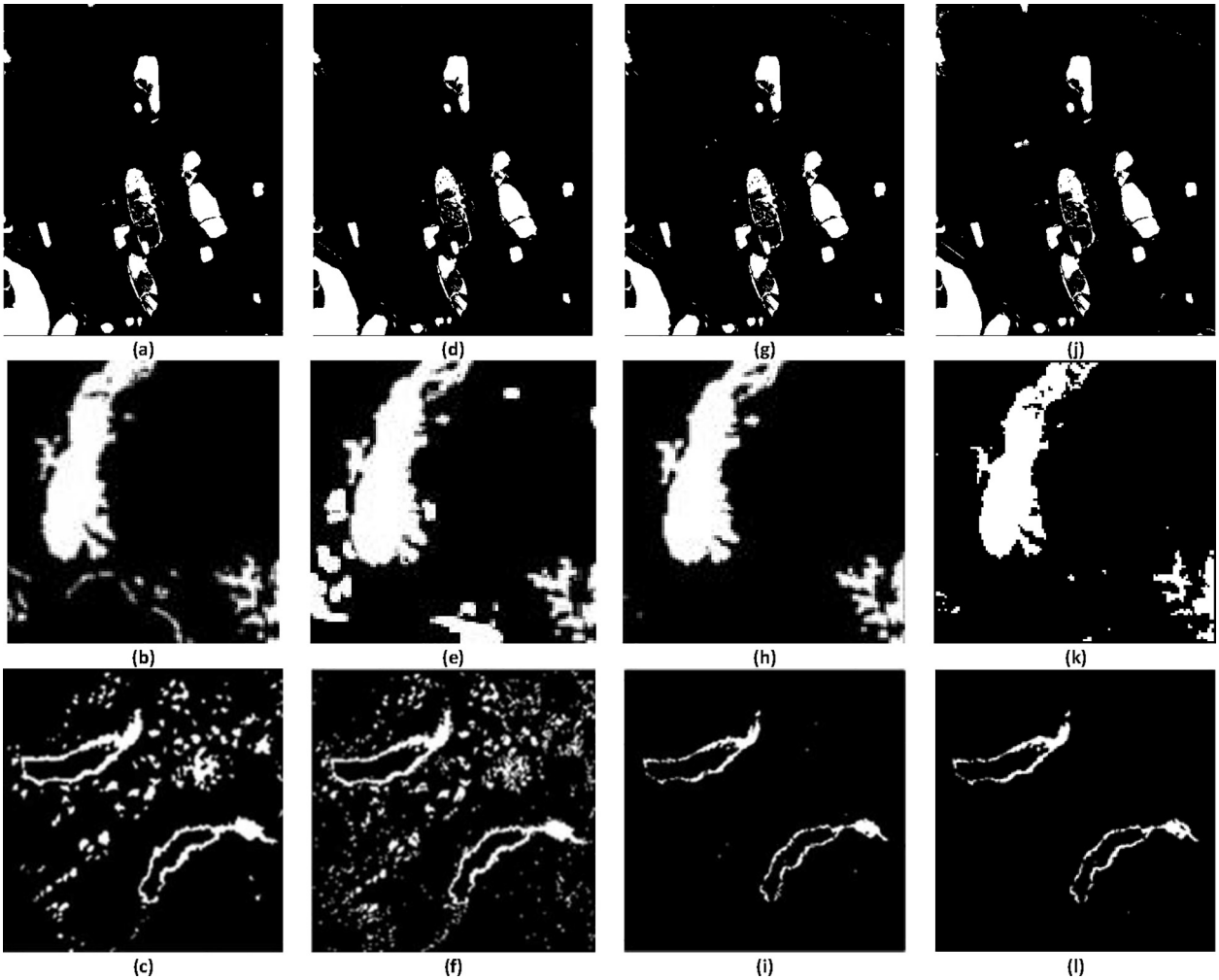

Fig. 5. Change map obtained using (a)-(c) EM algo (d)-(f) MRF algo (g) - (i) GMM method (j)–(l) Proposed Method.

Table 3
Result of various Parameters used for quantitative comparison.

Image	Method	TP	TN	FP	FN	OE (%)	CE (%)	OA (%)
Bangladesh	EM	9299	3049	173	4902	34.51	5.36	70.87
	MRF	10,066	3065	157	4135	29.11	4.87	75.36
	GMM	13,655	3101	121	546	3.84	3.75	96.10
	PM	14,065	3126	96	136	0. 95	2.97	98.66
Alaska	EM	14,082	160,531	2428	1827	11.48	1.48	97.62
	MRF	14,186	161,540	1419	1723	10.83	0.87	98.24
	GMM	14,915	162,108	851	994	6.24	0.52	98.96
	PM	15,577	162,334	625	332	2.08	0.38	99.46
Reno and Lake Tahoe	EM	992	62,167	1931	446	31.01	3.01	96.37
	MRF	1020	62,673	1425	418	29.06	2.22	97.18
	GMM	1259	62,876	1222	179	12.44	1.90	97.86
	PM	1314	63,010	1088	124	8.62	1.69	98.15

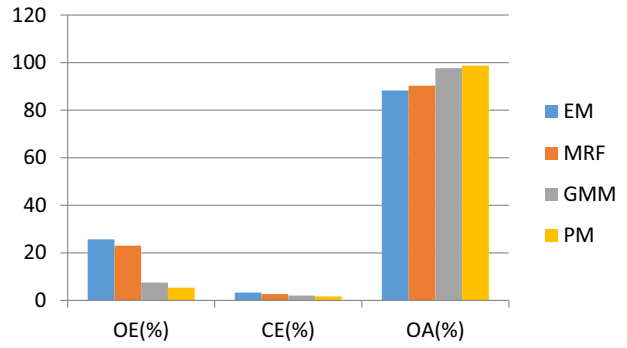

Fig. 6. Comparative Analysis.

the result of applying GMM based method. In this approach, the difference image is classified into change and unchanged classes using Bayes theory and Gaussian Mixture model (Celik, 2010).

Table 3 shows the quantitative analysis of the results. The omission error, commission error and overall accuracy for all the methods are computed. The average values of OE, CE and OA for the different methods are represented in Fig. 6.

4. Conclusion

This paper presented a novel method for change detection from satellite images based on statistical distribution and spectral features. The proposed method uses two indices, i.e., Spectral change index and similarity index for identifying changes. The spectral change index is computed using CVA which is good measure of change detection as it combines change information from multiple bands. But the spectral features may vary depending on the image acquisition conditions whereas the statistical distribution remains the same. The similarity index computes the divergence in the pdfs and this is obtained using KLD. The complementary change information obtained from these indices is combined using wavelet fusion rule to obtain complete change information. A change map is finally obtained by classifying the fused image into two classes changed and unchanged using the neuro fuzzy classifier RBF-GIFP/FCM The use of the neuro fuzzy classifier overcomes the mixed pixel problem and gives accurate change map. The proposed method was applied on three different data sets from different sensors and a comparative analysis of the proposed method with other existing state of the art methods is done. The results show that the proposed method has higher accuracy and low error values indicating the effectiveness of the proposed method. It is observed from the results that fusion of spectral and similarity measure is a good choice for change detection in images. In cases like natural disasters when the image acquisition conditions are extremely different the proposed method will give good results.

References

Bovolo, F., Bruzzone, L., Marconcini, M., 2008. A novel approach to unsupervised change detection based on a semisupervised SVM and a similarity measure. IEEE Trans. Geosci. Rem. Sens. 46 (7), 2070–2082.
Bovolo, F., Marchesi, S., Bruzzone, L., 2012. A framework for automatic and unsupervised detection of multiple changes in multitemporal images. IEEE Trans. Geosci. Rem. Sens. 50 (6), 2196–2212.
Bruzzone, L., Prieto, D.F., 2000. Automatic analysis of the difference image for unsupervised change detection. IEEE Trans. Geosci. Rem. Sens. 38 (3), 1171–1182.
Bujor, F., Trouvé, E., Valet, L., Nicolas, J.M., Rudant, J.P., 2004. Application of log-cumulants to the detection of spatiotemporal discontinuities in multitemporal SAR images. IEEE Trans. Geosci. Rem. Sens. 42 (10), 2073–2084.
Celik, T., 2010. Method for unsupervised change detection in satellite images. Electron. Lett. 46 (9), 624–626.
Çelik, T., 2011. Bayesian change detection based on spatial sampling and Gaussian mixture model. Patt. Recog. Lett. 32 (12), 1635–1642.
Celik, T., Ma, K.K., 2010. Unsupervised change detection for satellite images using dual-tree complex wavelet transform. IEEE Trans. Geosci. Rem. Sens. 48 (3), 1199–1210.
Celik, T., Ma, K.K., 2011. Multitemporal image change detection using undecimated discrete wavelet transform and active contours. IEEE Trans. Geosci. Rem. Sens. 49 (2), 706–716.
Chatelain, F., Tourneret, J.Y., Inglada, J., 2008. Change detection in multisensor SAR images using bivariate gamma distributions. IEEE Trans. Image Process. 17 (3), 249–258.
Du, P., Liu, S., Xia, J., Zhao, Y., 2013. Information fusion techniques for change detection from multi-temporal remote sensing images. Inform. Fus. 14 (1), 19–27.
Ertürk, A., Plaza, A., 2015. Informative change detection by unmixing for hyperspectral images. IEEE Geosci. Rem. Sens. Lett. 12 (6), 1252–1256.
Gong, M., Zhou, Z., Ma, J., 2012. Change detection in synthetic aperture radar images based on image fusion and fuzzy clustering. IEEE Trans. Image Process. 21 (4), 2141–2151.
Jia, L., Li, M., Zhang, P., Wu, Y., An, L., Song, W., 2016. Remote-sensing image change detection with fusion of multiple wavelet kernels. IEEE J. Selec. Topic. Appl. Earth Observ. Rem. Sens. 9 (8), 3405–3418.
Johnson, R.D., Kasischke, E.S., 1998. Change vector analysis: a technique for the multispectral monitoring of land cover and condition. Int. J. Remot. Sens. 19 (3), 411–426.
Li, X., Ling, F., Foody, G.M., Du, Y., 2016. A superresolution land-cover change detection method using remotely sensed images with different spatial resolutions. IEEE Trans. Geosci. Rem. Sens. 54 (7), 3822–3841.
Mehrotra, A., Singh, K.K., Nigam, M.J., Pal, K., 2015. Detection of tsunami-induced changes using generalized improved fuzzy radial basis function neural network. Nat. Hazard. 77 (1), 367–381.
Pohl, C., Van Genderen, J.L., 1998. Review article multisensor image fusion in remote sensing: concepts, methods and applications. Int. j. Rem. Sens. 19 (5), 823–854.
Singh, K.K., Nigam, M.J., Pal, K., Mehrotra, A., 2014. A fuzzy kohonen local information C-means clustering for remote sensing imagery. IETE Tech. Rev. 31 (1), 75–81.
Starck, J.L., Fadili, J., Murtagh, F., 2007. The undecimated wavelet decomposition and its reconstruction. IEEE Trans. Image Process. 16 (2), 297–309.
Zheng, Y., Zhang, X., Hou, B., Liu, G., 2014. Using Combined Difference Image and k-Means Clustering for SAR Image Change Detection. IEEE Geosci. Rem Sens. Lett. 11 (3), 691–695.